Monitoring horizontal movement of top of a spire in Saint Mary Cathedral of Burgos via computer vision

Miguel A. Vicente[1,*], Álvaro Mena[1], Jesús Mínguez[1], and Dorys C. González[1]

[1] Department of Civil Engineering, University of Burgos, c/Villadiego, s/n. 09001 Burgos, Spain.

* Correspondence: mvicente@ubu.es; Tel.: +34-947-25.94.23

Number of words: 6634
Number of tables and figures: 24

Keywords: horizontal movement, structural health monitoring, computer vision, historical heritage.

Abstract

Long-term monitoring of horizontal movement of the top of vertical elements, such as towers of historical monuments or chimneys, remains a challenge with current solutions. In such structures, which are usually of high historical and cultural value, ageing and structural degradation directly impact their horizontal movement.

This study presents a novel solution based on computer vision that allows the monitoring of horizontal movements with very good accuracy (uncertainty less than ±0.26 mm), high measurement speed (up to 5 Hz), and reduced cost.

A real-life validation was carried out on the south spire of the Saint Mary Cathedral in Burgos, Spain. Its horizontal movements were monitored for more than a year, and some relevant events were recorded, including high-range thermal variations, strong wind events, and ringing of the bells.

The results showed that the proposed solution was particularly robust for long-term monitoring of slow movements, such as those produced by thermal events or those derived from structural degradation. The white noise of the sensor was small and, for long-term measurements and small reading frequencies, it could obtain field accuracies of the order of ±0.1 mm at a recording frequency of 1/10 Hz, which further improved at lower recording frequencies.

1. Introduction

During the past decades, there has been a growing interest in the conservation of historical heritage, especially of religious structures (e.g., churches, cathedrals, and monasteries) as well as industrial buildings [1-7]. In general, such structures possess very complex geometries and use varied structural materials (e.g., stone, brick, and wood). In many cases, their historical and heritage value, and their social and economic importance are very high. However, the costs of repair or reconstruction can be very high as well, especially if the work is carried out late, i.e., when the structural damage is more than evident. In addition, this type of work is often very complex owing to the need to preserve the splendour of the building. For example, it is often essential to use the same materials and even the same construction techniques as were used when the structure was built.

Monitoring of unique structures and those that are particularly vulnerable is a very attractive strategy, as it can help determine the state of the structure in real-time and plan more accurate preventive maintenance actions, which are much more economical. However, monitoring such structures is a difficult task. Firstly, the design of a sensor network is complex owing to their structural complexity. Numerous types of sensors (accelerometers, inclinometers, strain gauges, thermocouples, etc.) can be arranged in different locations. In addition, the complexity of data analysis and post-processing grows exponentially with the number of sensors, which renders decision-making more difficult. This often leads to shelving of the monitoring of these unique constructions [8-13].

In the case of historic buildings with tall vertical elements, such as towers or spires in churches, cathedrals, minarets, and chimneys, monitoring could be significantly simplified because, in general, most of the pathologies in these buildings that could lead to their collapse cause horizontal movement of the top of the vertical element. Thus, for example, a differential settlement in the foundation of the building leads to a rotation of the tower and, consequently, a horizontal movement at the top of the building. In addition, if one of the load-bearing walls of the building partially sinks, it would lead to a rotation of the tower and a consequent horizontal movement of the top of the tower [14-20].

The horizontal movement of the top of a tower or spire in a historic building can be a good indicator of the structural health of the entire building, especially when its value is found to be outside the range typically produced by environmental conditions.

However, a technical challenge is how to monitor this horizontal movement accurately, for which the measurement system should possess the following essential characteristics:

1. Accuracy of the system to be able to provide sub-mm accuracy.
2. Robustness to withstand varying temperatures and humidity, and operate in harsh conditions.
3. Low invasiveness, especially for monitoring buildings of high historical value.

4. Possibility of autonomous data collection to reduce on-site labour costs.
5. Reliability to yield accurate and repeatable measurements.
6. Low cost owing to the large number of historic buildings to be monitored.

There are currently some technical solutions on the market, such as laser distance meters, laser interferometers, total stations, global positioning system (GPS)-based systems, geophones, and accelerometers. However, none of them can meet all the desired requirements.

Up to date, most of the research work related to the monitoring of these vertical elements focuses on the study of their dynamic response, instead of their static response. However, the information it provides used to be insufficient and it is often not useful enough for making decisions related, for example, to the need or not to carry out an urgent structural repair [21-25].

In recent years, a new technology has emerged, based on computer vision. The development of this technology has been progressing very fast, driven by a continuous improvement of the characteristics of digital video cameras, which has resulted in rapidly decreasing costs. Simultaneously, the increase in the computing power of computers makes it possible to analyse images in real-time [26-33].

Within this field, the work developed by Vicente et al. [34, 35] is noteworthy. They developed a system, namely a laser and video-based displacement transducer (LVBDT), which is based on the combined use of a laser (typically one or two laser beams), which acts as a fixed reference, and a video camera to monitor the movements (Figure 1).

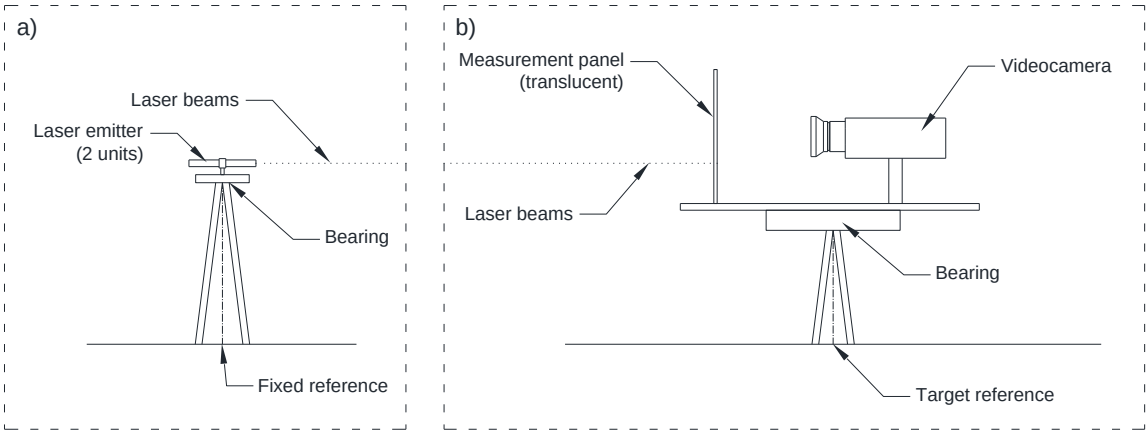

Figure 1. LVBDT: a) fixed part and b) movable part [35].

This system has been tested to date on a few bridges and a building; however, measurements of short duration (lasting only a few minutes) only have been carried out. The above-mentioned studies have established the feasibility of this technology. However, to date, it has not been tested in a real environment over a long time; furthermore, It has never been used to monitor movements in a historic building.

There are a few examples in relevant literature on drift monitoring of vertical elements (such as towers, spires, and minarets). In this context, some techniques are available that allow the detection of these movements. One of them is terrestrial laser scanning (TSL) [36]. This solution provides interesting data; however, it is less accurate and more expensive than the one presented in this work. Another solution is photogrammetry [37, 38]; even though it is a low-cost solution, it suffers from an important uncertainty in that its sampling frequency is very low.

This study demonstrates the monitoring of the south spire of the Cathedral of Saint Mary of Burgos, Spain, carried out intermittently for more than a year, to test the LVBDT sensor, described in detail in [34, 35], in a real environment over a long period of time.

The remainder of this article is structured as follows. Section 2 describes the monitored structure and the monitoring technology solution adopted, which included an LVBDT sensor and other conventional sensors. Section 3 presents the results obtained from the data recorded during certain environmental events. Finally, a summary and conclusions are presented in Section 4.

2. Description of the sensor

The sensor used in this project is very similar to the one described in [34, 35], with some differences as described below.

Firstly, the fixed part of the system consisted of a single laser emitter because the objective was to monitor only the displacements; therefore, a single device was sufficient. The emitter used was a laser module (FP-LR-250-25-C-F, Laser Components GmbH, Olching, Germany). It was a green diode laser with a wavelength of 520 nm and an output power of 25 mW. The laser was powered by a 220-V alternating current. Additionally, it was fixed to the needle wall by means of a precision holder (FP-MP-30, Laser Components GmbH, Olching, Germany) (Figure 2).

Figure 2. Laser emitter.

Secondly, the moving part was made up of several elements. These included a translucent 85 × 85 mm panel, on which the laser spot would hit. On the inner side of this panel, there were two red LEDs 100 mm apart such that they would define a reference direction to monitor the displacements. The LEDs were powered by a 12 V DC current.

Furthermore, both the LEDs and the light spot emitted by the laser were visualised using a video camera (Logitech Brio, Lausanne, Switzerland), measuring 27 × 102 × 27 mm and capable of 4K resolution (4096 × 2160 px) and a shutter speed of 30 fps. The distance between the webcam lens and panel was 130 mm. In addition, a filter was placed over the camera lens to improve detection (Figure 3).

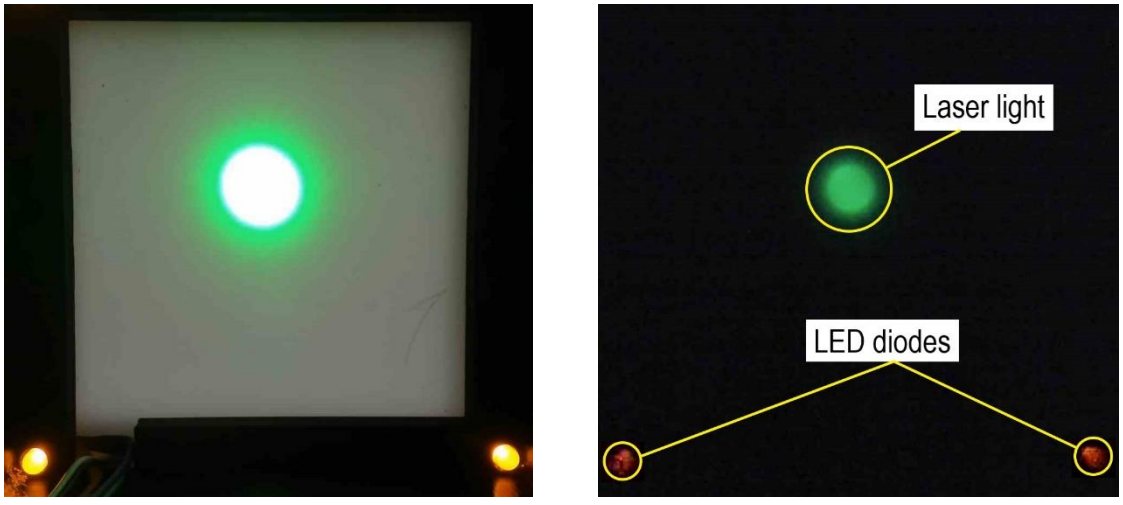

(a) (b)

Figure 3. Image filtering using an inactinic welding glass: (a) original image and (b) filtered image.

Finally, the camera and translucent panel were housed in a plastic box, creating a compact, weather-protected unit. This box was designed specifically for this purpose and manufactured from acrylonitrile butadiene styrene (ABS) using a 3D printing device (Ultimaker S3, Utrecht, Netherlands) (Figure 4).

Figure 4. 3D printed box containing camera and translucent panel.

The video camera was connected to a computer, and the data were analysed in real-time using a MATLAB algorithm (MathWorks, Natick, Massachusetts, USA) developed by the authors. The input data were the frames captured by the camera, which were processed at a rate of 5 Hz. It should be noted that the camera was previously calibrated to eliminate any distortion. To this end, a procedure very similar to that described by Brown et al. [34] was followed. Consequently, the frames processed by the algorithm were corrected using the calibration parameters of the video camera.

Figure 5 shows the implemented algorithm, which is further described below. First, the RGB images of each frame were transformed into grayscale images. Second, to discretise the three light sources, a threshold grey value was set so that those pixels whose values were lower than this threshold were considered "background" while those, whose values were higher, were considered "light sources". This process is called binarisation, as the pixels that make up the image can only have two values: 0 (black) or 1 (white). In this case, considering that the greyscale images were 8-bit (i.e., the greyscale ranges from 0 to 255), the threshold value was set to 10. Therefore, the pixels with a grey value in the range 0–10 were considered "background", while those with a value in the range 10–255 were considered "light sources".

Third, all the pixels that were part of the same light source were merged. The proximity criteria were used for this purpose. Next, the coordinates of the centroids of each light source were determined, taking one of the LEDs as the origin of the coordinate system. In this way, the coordinates of the laser spot, measured in pixels, were obtained directly. The X- and Y- coordinates of the centroid of each light source were determined as the mean value of the X- and Y- coordinates of the pixels that belonged to that light source.

Finally, to transform the pixels into mm, a scale factor was calculated, considering that the real distance between the centroids of the two LEDs was 100 mm. This process was repeated for each frame. In addition, the algorithm contained filtering tools to eliminate digital noise in the images. More detailed information can be found in Brown et al. [34].

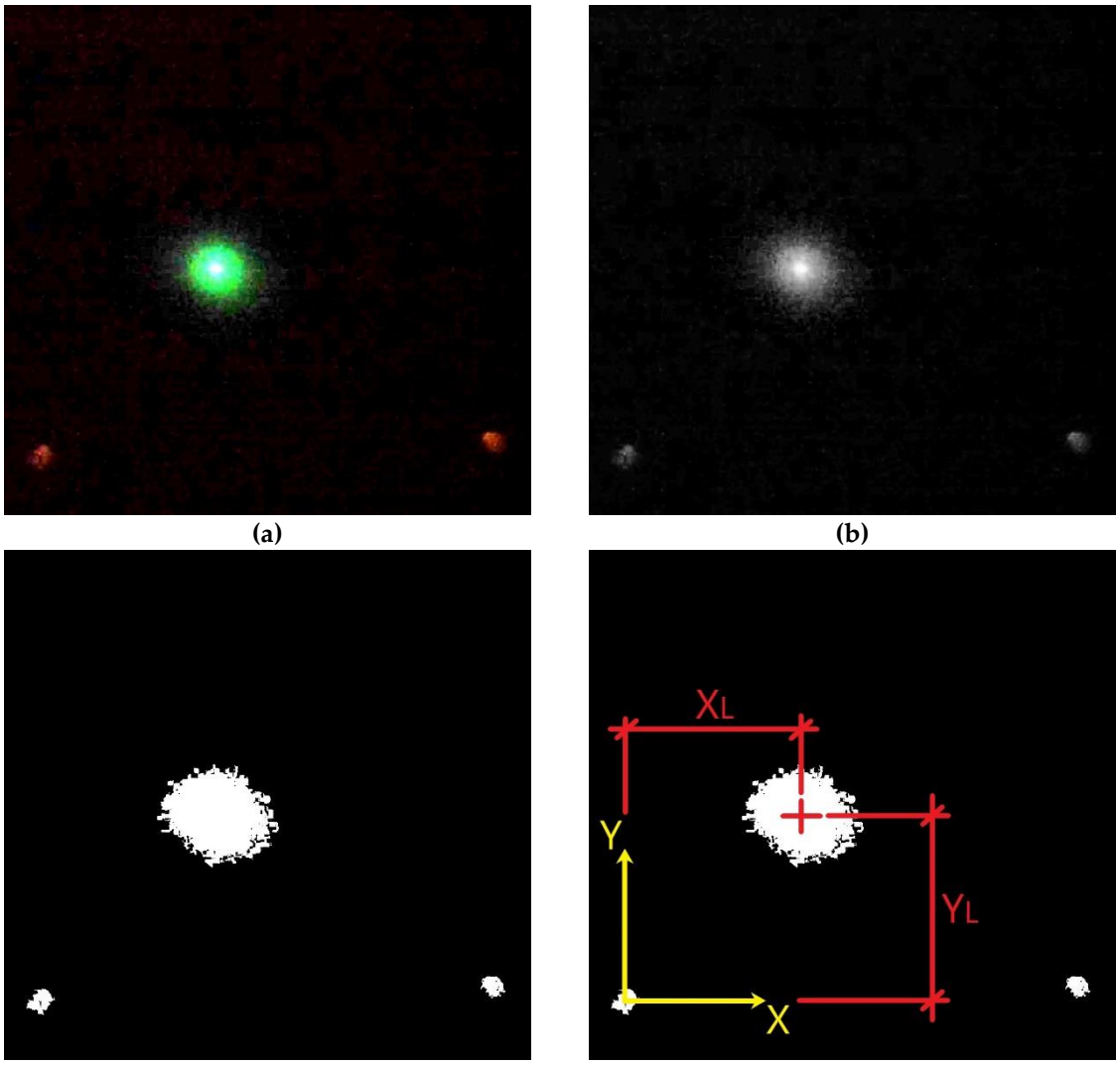

Figure 5. Algorithm description: (a) original frame, (b) grayscale image, (c) image binarisation, and (d) extraction of laser spot centroid coordinates.

This solution is very robust to changes in light conditions and they do not affect the measurement [34]. Convective air currents can slightly modify the laser trajectory and this may explain some of the measured white noise. There are also other effects that can also cause white noise, such as the internal vibration of the laser emitter.

3. Experimental campaign

3.1. Description of the Cathedral of Burgos

During the years 2020 and 2021, the south spire of the Cathedral of Saint Mary of Burgos, Spain was monitored intermittently (Figure 6). This is a Catholic church, dedicated to Virgin Mary. Its construction began in 1221, following French Gothic patterns. Its construction lasted over 500 years. A variety of architectural styles, can be clearly seen in the church, ranging from an early Gothic in the first part of the work to the later Gothic in the latest extensions. Today, it is a fine example of Gothic architecture in Europe and was declared a UNESCO World Heritage Site in 1984. In 2021, the eighth centenary of the beginning of its construction was commemorated.

Figure 6. General view of the Cathedral of Saint Mary of Burgos, Spain.

The two spires on the façade of Santa María (Figure 7) stood out for their height. These elements date back to the 15th century and were designed by the German architect Johannes von Köln (Cologne, Germany, 1410 – Burgos, Spain, 1481).

Figure 7. General view of the south spire placed on the façade of Saint Mary Cathedral.

The temple is now in an excellent state of conservation, particularly the spires. Therefore, it is a suitable infrastructure for testing the proposed system for monitoring horizontal movements based on computer vision.

3.2. Testing equipment

The LVBDT sensor described earlier was used to monitor the horizontal movements of the southern spire. All the components of the sensor were installed inside the spire so that they were partially protected from the weather. The laser emitter was located at the base of the spire, where it is assumed that there is no rotation or displacement, while the translucent panel and video camera were located at the top of the spire (Figure 8). The distance between the laser emitter and the translucent panel was 22.2 m.

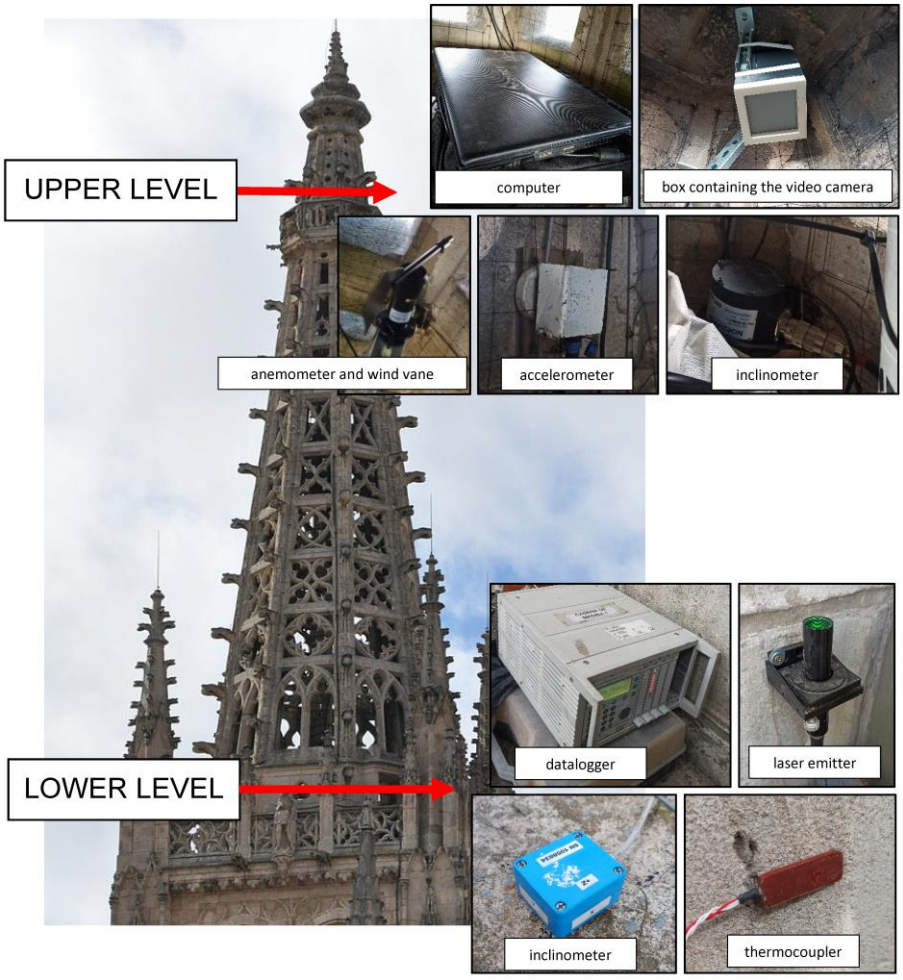

Figure 8. General scheme of the sensors and devices placed in the spire.

Additionally, conventional sensors were used (Figure 8). A biaxial inclinometer model (PST300, PEWATRON AG, Zürich, Switzerland), with a measuring range of ±5º and an absolute accuracy of ±0.01°, was installed in the lower part. Furthermore, a PT100 thermocouple was mounted on the lower part of the spire to monitor the ambient temperature.

At the top of the spire, the following sensors were installed: A biaxial inclinometer (PST300, PEWATRON AG, Zürich, Switzerland); a triaxial accelerometer (4630, TE Connectivity, Ltd., Schaffhausen, Switzerland), with an acceleration range of ±2g, a frequency range of 0–700 Hz, and a sensitivity of 1000 mv/g; and an anemometer coupled with a wind vane to monitor wind speed and direction.

All conventional sensors were connected to a datalogger (MCGPlus, HBM, Darmstadt, Germany) and a laptop computer. In addition, a video camera was directly connected to the computer so that using the algorithm described earlier, the movements of the top of the spire could be evaluated in real-time (Figures 9 and 10).

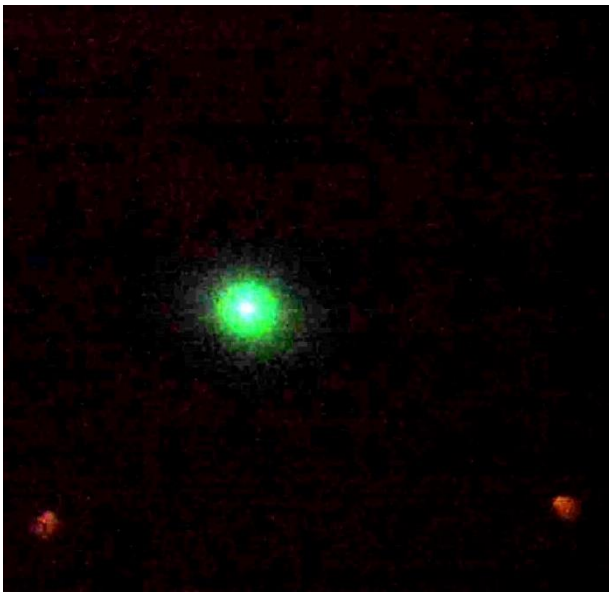

Figure 9. Typical image captured by the camera at a specific instant.

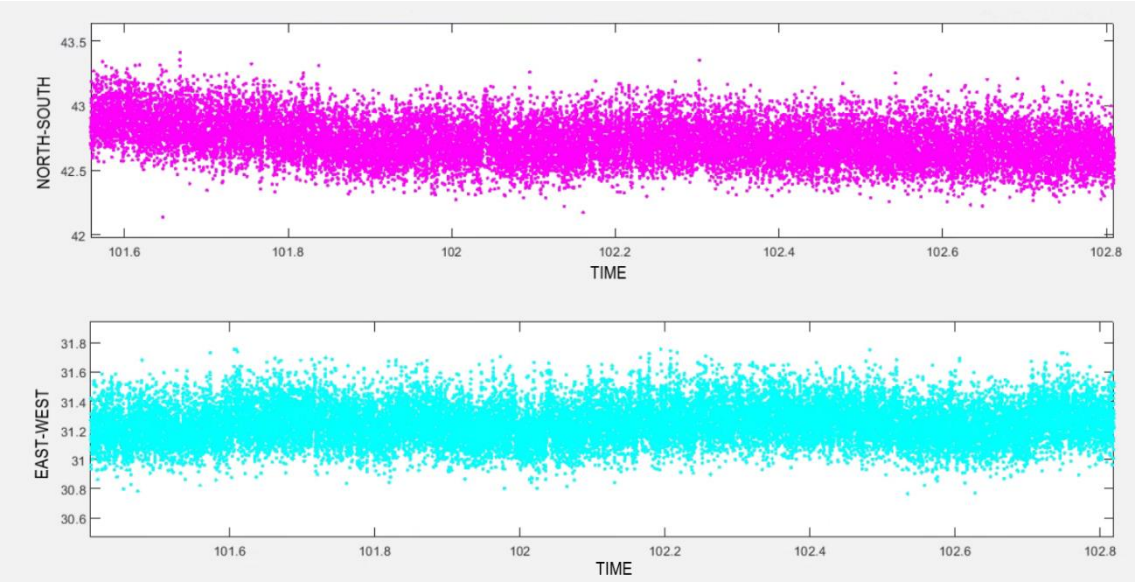

Figure 10. Real-time plotting of graphs with north–south (top) and east–west (bottom) movements. X- axis in seconds, Y- axis in millimetres.

3.3. Description of the monitoring process

Monitoring was carried out intermittently in 2020 and 2021. Short measurements, lasting a few days, and longer measurements, lasting several months, were performed. During this time, some relevant meteorological events were monitored, which are described below.

1. Thermal variation event. The response of the needle was monitored during 29–31 March, 2021, when the daily thermal variations were particularly relevant.

2. Wind event. The response of the needle was monitored during the wind storm that took place during 20-21 March, 2021, with gusts reaching close to 60 km/h.

3. Induced vibration event. The response of the spire was monitored during the ringing of bells, which lasted 3 min on 25 May, 2021 at 6:55 PM.

Furthermore, to check the robustness of the sensor, a measurement stability test was carried out by comparing the measurements on two meteorologically similar days spaced more than one month apart. Finally, a test was performed to estimate the white noise of the laser sensor.

In each of these events, all the sensors arranged on the spire were recorded. The reading frequency of the LVBDT was 5 Hz, and that of the other conventional sensors was 20 Hz.

3.4. Numerical simulation

Additionally, a model of the spire of the cathedral was developed using the finite element method (FEM) to estimate the horizontal movements of the top from the data provided by the conventional sensors, namely the anemometer, wind vane, and thermocouple.

The spire was modelled based on the historical construction drawings supplied by the Cathedral Chapter. Tetrahedral solid elements of quadratic order were used, with a maximum size of 100 mm. In total, the model consisted of 2.42×10^5 elements. Figure 11 shows the geometry of the spire and mesh.

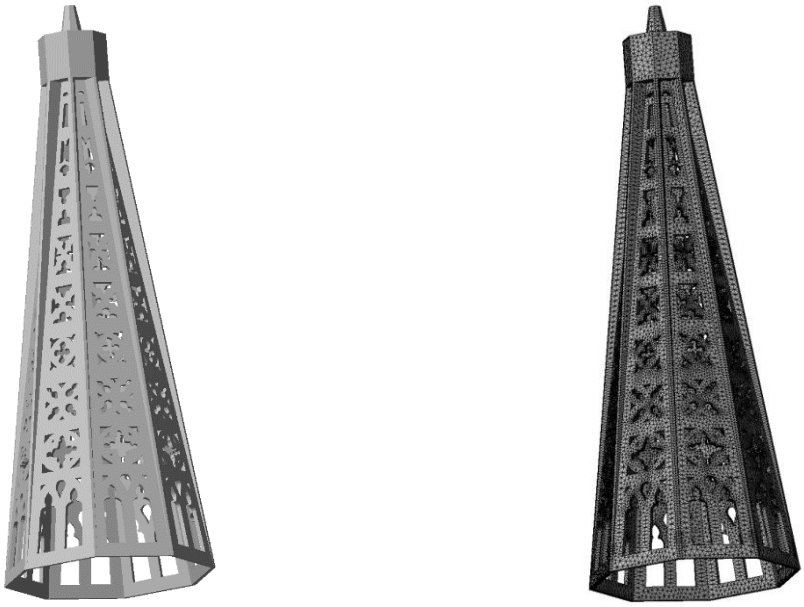

(a) (b)

Figure 11. Finite element model of the spire: (a) geometry and (b) mesh.

The boundary conditions imposed on the model consisted of a fixed support (to prevent displacements in X-, Y-, and Z- directions) throughout the base, thus simulating the connection of the spire with a much more rigid element, such as the rest of the Cathedral tower.

The Cathedral was built with limestone from the quarries of Hontoria and Cubillo del Campo, located approximately 100 km southwest of Burgos.

This limestone was from the Turonian–Campanian period and is not very crystalline; it is dull, very uniformly white, pure, massive, and homogeneous; it has a very fine saccharoidal appearance and is classified as a very pure packstone limestone containing some fossils (echinids, milliolids, and rudists). It is of sedimentary origin and belongs to rudist facies. It is mostly micritic, which allows for better weathering.

Table 1 lists the physical parameters considered in the numerical models [39-41].

Table 1. Main parameters of limestone considered in the numerical models.

Parameter	Value
Density (kg/m^3)	2200
Thermal conductivity (W/m°C)	2.2

Thermal expansion coefficient (°C^{-1})	1.40×10^{-5}
Modulus of elasticity (GPa)	30
Poisson's coefficient	0.18

4. Results

The results obtained for each of the events described above as well as their correlation with the numerical models employed, are discussed below.

4.1. Estimation of the white nose of the sensor

In the early morning of 23 February, 2021 a one-hour monitoring was carried out (between 2:00 AM and 3:00 AM), during which the environmental conditions were very stable. The temperature was particularly stable in this time slot, with a mean value and maximum variation of 4 and 0.3 °C, respectively. There was a light, steady, south-westerly wind with a wind speed between 4 and 8 km/h. Therefore, the environmental conditions were ideal for evaluating the white noise of the LVBDT sensor.

Figure 12 shows the horizontal movements at the top of the spire. As indicated above, the sampling rate was 5 Hz (Figure 12a). Figure 12b shows the average horizontal movements per second, which were obtained by calculating the average value of five recorded data points. Figures 12c and 12d show the mean values every 10 s and 1 min, respectively.

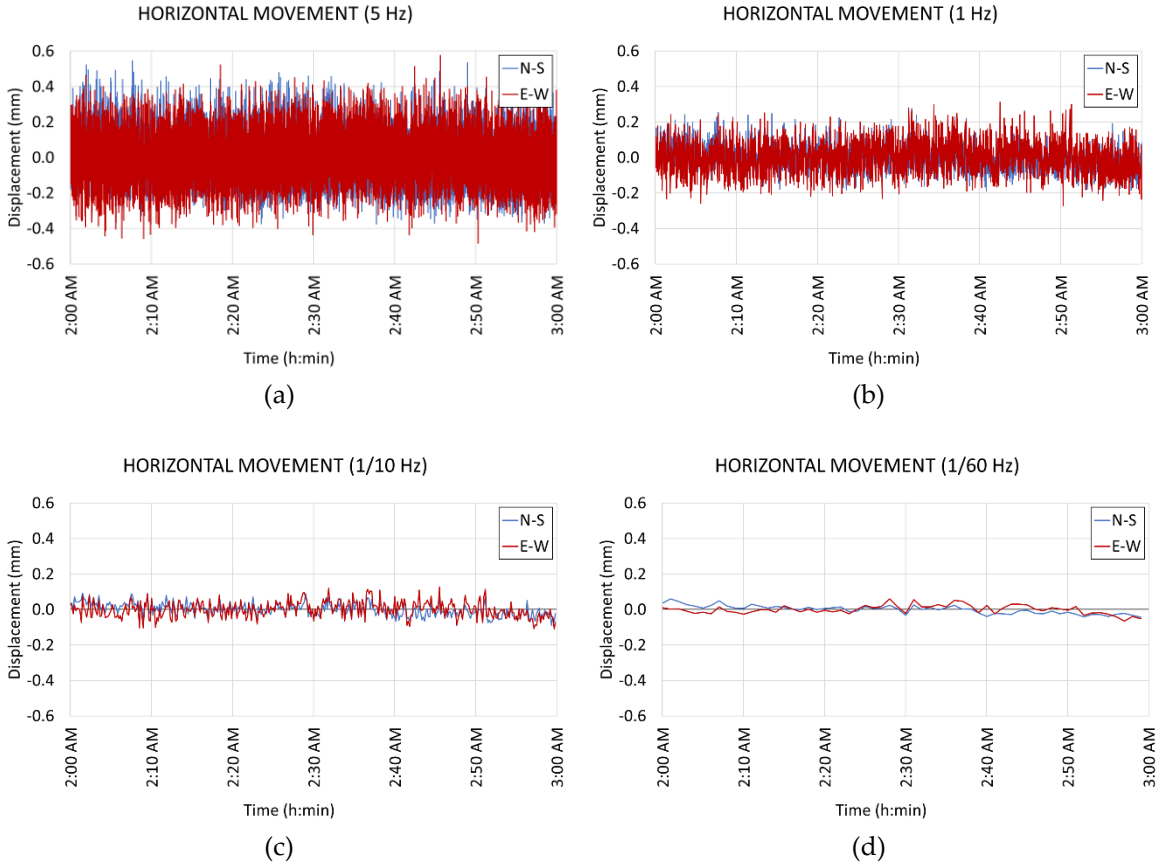

Figure 12. White noise at different recording frequencies (Hz): (a) 5, (b) 1, (c) 1/10, and (d) 1/60.

Additionally, A DFT was performed on the data recorded by the LVBDT to verify that the signal is white noise (Figure 13).

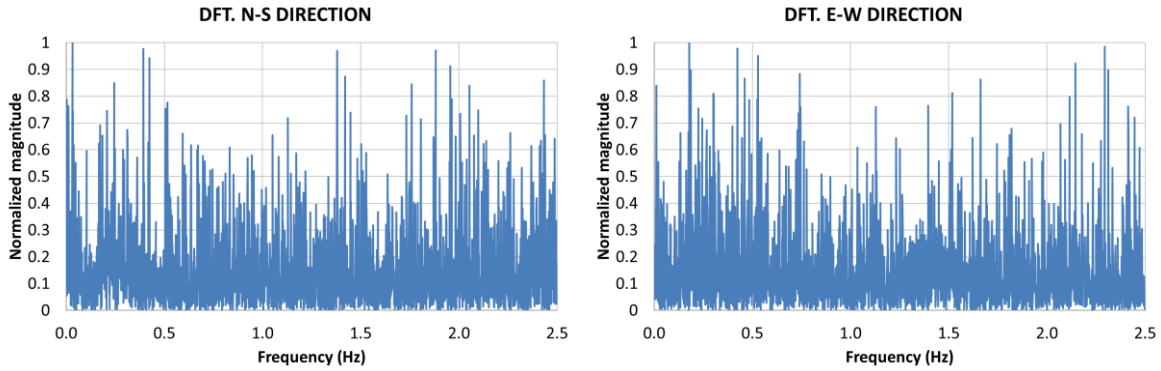

(a) (b)

Figure 13. DFT results from the LVBDT: (a) North-South direction, and (b) East-West direction.

Figure 13 demonstrates that the signal is white noise, since there is no dominant frequency within the analyzed range.

White noise, which is stochastic in nature, was considerably reduced when the average values of longer time periods (lower recording frequencies) were considered. Therefore, as can be seen in Figure 12, the longer the time period considered, the lower the dispersion of the data. Table 2 shows the mean values (the measurement was set to zero at the beginning of the test), standard deviation, and confidence intervals of the measurement for both north–south and east–west orientations.

Table 2. Statistical parameters of the white-noise event.

Direction	Statistical parameters (in mm)	Recording frequency (Hz)			
		5	1	1/10	1/60
N-S	μ	0.00	0.00	0.00	0.00
	σ	0.13	0.09	0.05	0.03
	Confidence interval 95%	[0.26,–0.26]	[0.17,–0.17]	[0.09,–0.09]	[0.05,–0.05]
E-W	μ	0.00	0.00	0.00	0.00
	σ	0.12	0.07	0.04	0.02
	Confidence interval 95%	[0.24,–0.24]	[0.14,–0.14]	[0.07,–0.07]	[0.05,–0.05]

As summarised in Table 2, the confidence interval decreased with the recording frequency. For the case of the highest frequency (5 Hz), the maximum uncertainty occurred in the north–south direction and was ±0.26 mm. In contrast, for the lowest frequency (1/60 Hz or 1 data/min), the measurement uncertainty was ±0.05 mm.

In the case of monitoring horizontal movements caused by slow phenomena (such as ageing or mechanical degradation), the best results would be obtained considering a sampling frequency of 5 Hz and recording the average values at 1/60 Hz. Thus, the highest measurement accuracy could be achieved.

However, in this study, a sampling frequency of 5 Hz was considered for the LVBDT, and then the average value was considered every second. This option also provided good accuracy.

4.2. Thermal variation event

A representative thermal variation event took place during 29-31 March, 2021. Figure 13 shows the measurements recorded by the most significant sensors, namely temperature, wind speed, tilt, and horizontal movements of the top of the spire.

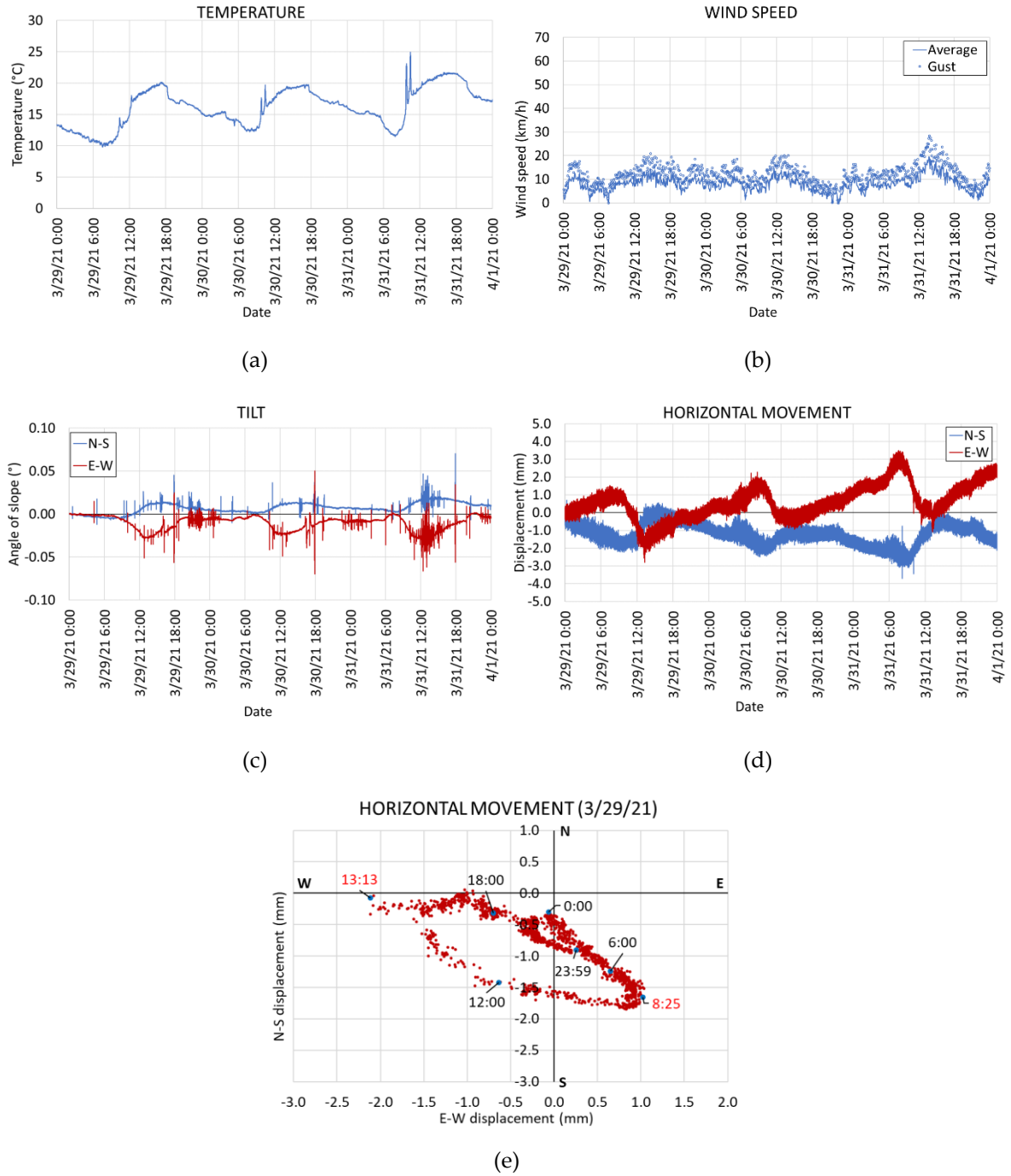

Figure 13. Measurements during the thermal variation event on 29 March 2021: (a) temperature, (b) wind speed, (c) tilt, (d) horizontal movement, and (e) horizontal movement according to the cardinal axes.

As shown in Figure 13a, during this period, the daily thermal oscillation, defined as the numerical difference between the maximum and minimum temperature values, was approximately 10 °C. It is noteworthy that the exceptional temperature peaks occurring every day at approximately 10:00 AM (especially on 31 March) were not real. This is explained by the fact that during that time, the thermocouple received direct sunlight, which abnormally increased the recorded values. Therefore, they were not considered in the evaluation of the results.

Figure 13b shows the average wind speed during the event, including the gusts. It can be seen that the mean wind speed remained approximately constant, with values always below 20 km/h. This is important because the wind had an insignificant impact on the results measured by the LVBDT sensor.

Figure 13c shows the inclinations at the top of the spire. Clearly the tower tilt oscillations were of thermal origin. The highest inclinations occurred during the middle hours of the day when the solar radiation was the highest. On the other hand, the minimum values were obtained during the night, when the temperature was lower. The average maximum inclinations during the event in the north–south and east–west directions were 0.03 and 0.05°, respectively. Therefore, it can be concluded that the direction of the needle tilt was approximately east–west.

On the other hand, Figure 13d shows the displacements at the top of the spire, as measured by the LVBDT. Again, it was observed that the thermal variations had a determining influence, as the plots were practically homothetic to those in Figure 13a. The maximum variations measured during this event in the north–south and east–west directions were approximately 2 and 4 mm, respectively. These results agreed with those recorded by the inclinometer, confirming that there was a rotation of the spire in the east–west direction. However, there was a fundamental difference between the two sensors. While the inclinometer could hardly detect the thermal movements of the structure during the night (9 PM to 8 AM), the LVBDT could. This shows that this novel sensor possessed a high sensitivity under these circumstances.

When the temperature and horizontal displacements were superimposed, a clear correlation could be obtained (figure 14).

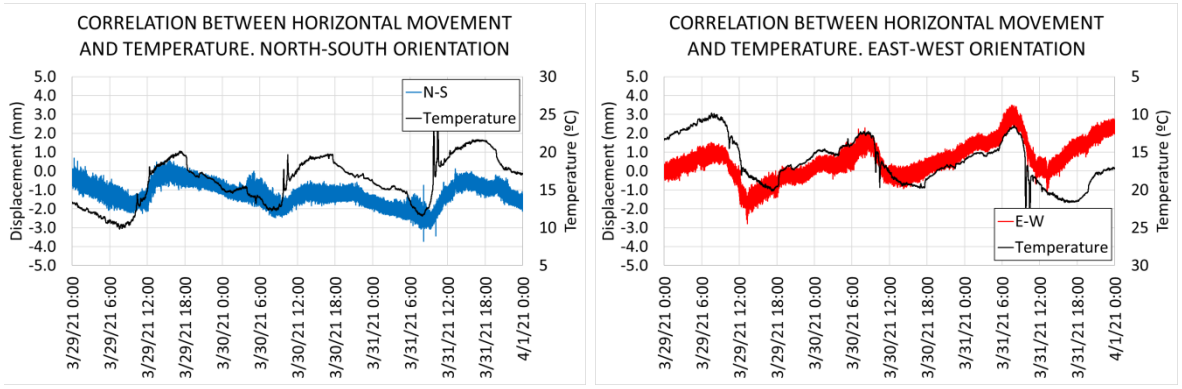

(a) (b)

Figure 14. Correlation between horizontal movement and temperature: a) north–south orientation and b) east–west orientation.

In summary, the thermal variations experienced by the spire caused a horizontal movement at its top as well as rotation. As observed, the horizontal movements were of the order of a few mm, while the rotation was only of a few hundredths of a deg. The LVBDT sensor, which had an accuracy of approximately ±0.2 mm for a sampling rate of 1 Hz (see Table 2), could accurately measure movements of a few mm. However, the inclinometer, which had an accuracy of ±0.01°, did not adequately record rotations of a few hundredths of a deg.

For a better understanding of the daily rotation of the top of the spire, this movement could be represented in terms of the cardinal axes. Figure 13e shows the spatial motion of the needle on 29 March, 2021. The results clearly reveal that the predominant motion was along the east–west direction, again coinciding with the inclinometer data. Furthermore, the westward tilt occurred during the period of the highest solar radiation, which in this case, was between 8:25 AM and 1:13 PM. During this period, the greatest increase in temperature occurred (Figure 13a). On the other hand, the eastward tilt slowly recovered during the afternoon and evening, coinciding with the decrease in the temperature.

Figure 15 shows the correlation between the tilt of the tower and its horizontal movement.

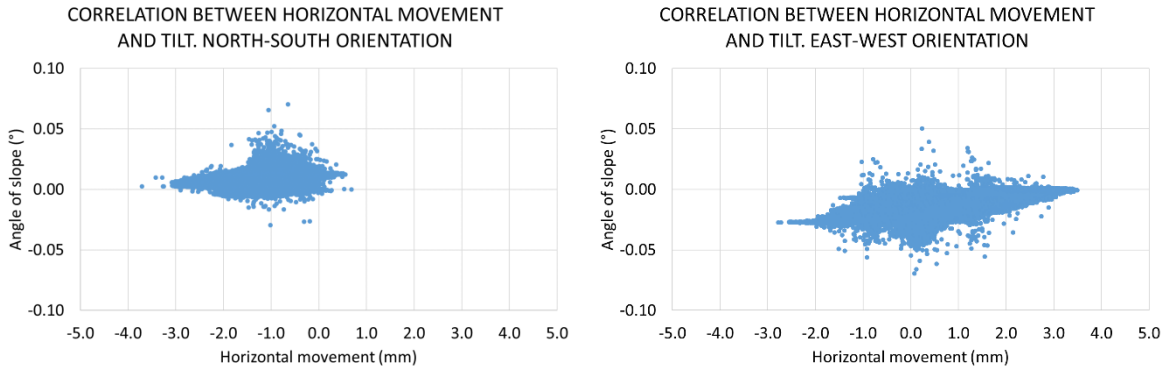

(a) (b)

Figure 15. Correlation between horizontal movement and slope: a) north–south orientation and b) east–west orientation.

In both the north–south (Figure 15a) and east–west directions (Figure 15b), a clear relationship between both the parameters was observed, which was understandable from a structural point of view. In both the cases, the fitting curves were noticeably horizontal, which meant that small turns were correlated with large horizontal movements. Given the technical characteristics of both the inclinometer and LVBDT, it was found that the latter was more sensitive than the former.

In addition, a numerical model was employed to estimate the horizontal movement of the top of the spire owing to the measured thermal variation. This model included some simplifications. Firstly, a thermal study was carried out to characterise the temperature distribution owing to the solar radiation on the surface of the spire. This study was of a stationary nature, that is, assuming permanent radiation from the south direction, without considering the rotation of the sun. Convective thermal transmittance with the air surrounding the structure of 10 W/m^2K was applied at an outside temperature of 20 °C, based on the maximum temperatures recorded by the thermocouple (Figure 13a). Consequently, it was determined that the solar radiation produced an input of 300 W/m^2 on the south side, which decreased to 100 W/m^2 on the east and west sides, and to zero on the north side.

Second, using the results of the thermal study as input data, a mechanical model was created to determine the magnitude of the movements at the head of the spire (Figure 16).

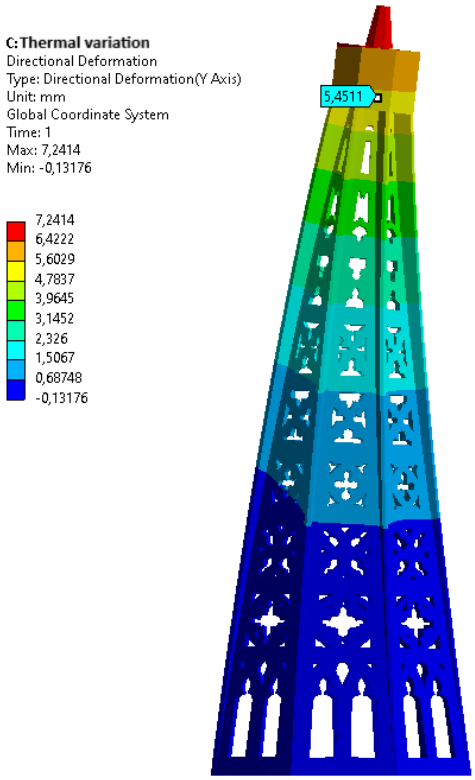

Figure 16. Horizontal movement of the spire due to thermal variations as obtained from the FE model.

The numerical model predicted that the maximum horizontal movement at the point where the LVBDT sensor was located was approximately 5.45 mm. This value could be compared with the maximum displacement that occurred at the top of the spire during the thermal variation event; i.e., in Figure 13e, the difference between the two extreme positions (corresponding to 8:25 and 13:13). The result was 3.51 mm; therefore, it could be concluded that the FEM model fit the experimental results considerably, taking into account the assumptions and simplifications made.

4.3. Wind event

For the wind event, the response of the spire was monitored during a storm that started in the afternoon of 20 March and ended late on 21 March, 2021. The wind direction was predominantly northeast. The parameters recorded during the wind event are displayed in Figure 17.

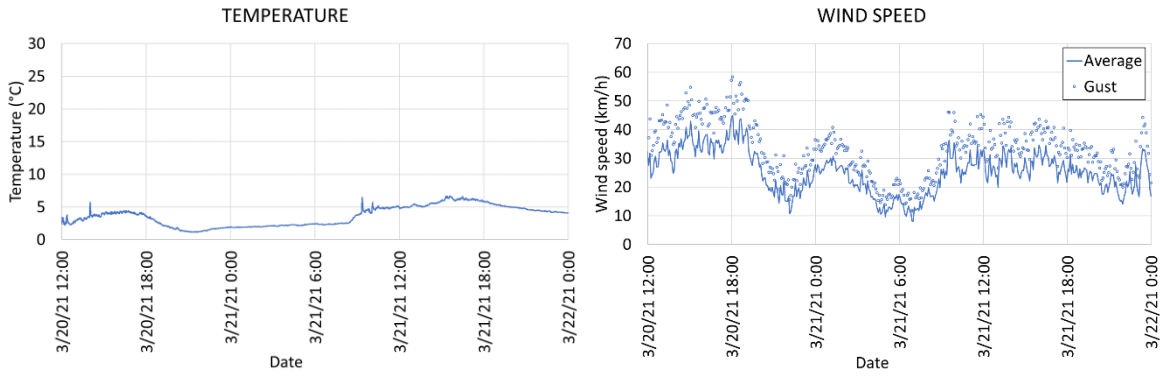

(a) (b)

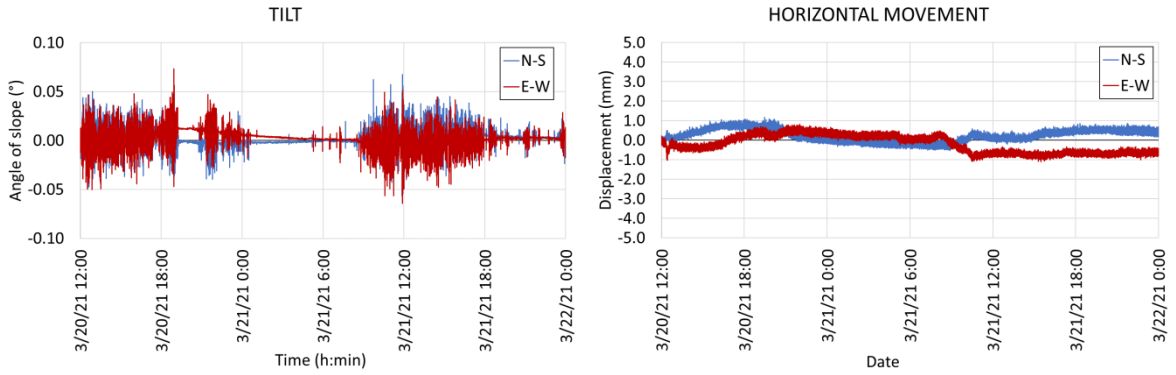

(c) (d)

Figure 17. Measurements during the wind event: (a) temperature, (b) wind speed, (c) tilt, and (d) horizontal movement.

As can be observed from Figure 17b, the highest wind gusts occurred during the afternoon of 20 March, 2021, reaching an average value of approximately 50 km/h. Specifically, an extreme gust occurred at 6:04 PM, with a value of 58.4 km/h. 21 March was considerably less windy, with gusts of approximately 40 km/h, which further decreased as the day progressed. As for the temperatures (Figure 17a), the temperature oscillation on 21 March was 4.7 °C. This was a relatively low value; although it would not eliminate the effects of thermal variations, it reduced them, as the focus in this case was on the wind.

The tilt at the top of the spire is shown in Figure 17c. The graph shows how the largest oscillations occurred during periods of highest wind. The movements that occurred were high-frequency vibrations of a dynamic nature, without a dominant direction and with an amplitude in terms of inclination of approximately ±0.07°. However, there was no correlation between the thermal variations and tilt. In this case, the effect of temperature, which caused much slower and continuous movements, was overshadowed by the action of the wind.

Finally, Figure 17d shows the horizontal displacement of the top of the spire monitored by the LVBDT. In this case, no horizontal movement was observed. The maximum horizontal movement was approximately 2 mm in both north–south and east–west directions. Furthermore, there was no correlation between the wind speed and horizontal movement. In contrast, there was a stronger correlation between the temperature variation and horizontal movement. In contrast to the inclinometer, the LVBDT recorded the low-frequency movements better; however, it could not record the high-frequency movements (i.e., those above 5 Hz in this case, which are typically caused by wind).

The main conclusion from this test was that the LVBDT is especially useful for measuring low- or very low-frequency displacements, for example, thermal, rheological, and structural ageing effects.

In addition, a numerical model was developed to estimate the theoretical values of the horizontal motion of the spire head. Firstly, a computational fluid mechanics (CFD) model was developed, considering a uniform wind flow with a velocity of 60 km/h, which approximately coincided with the maximum wind values recorded during the wind event (Figure 17b). Figure 18 shows key results from the CFD model employed.

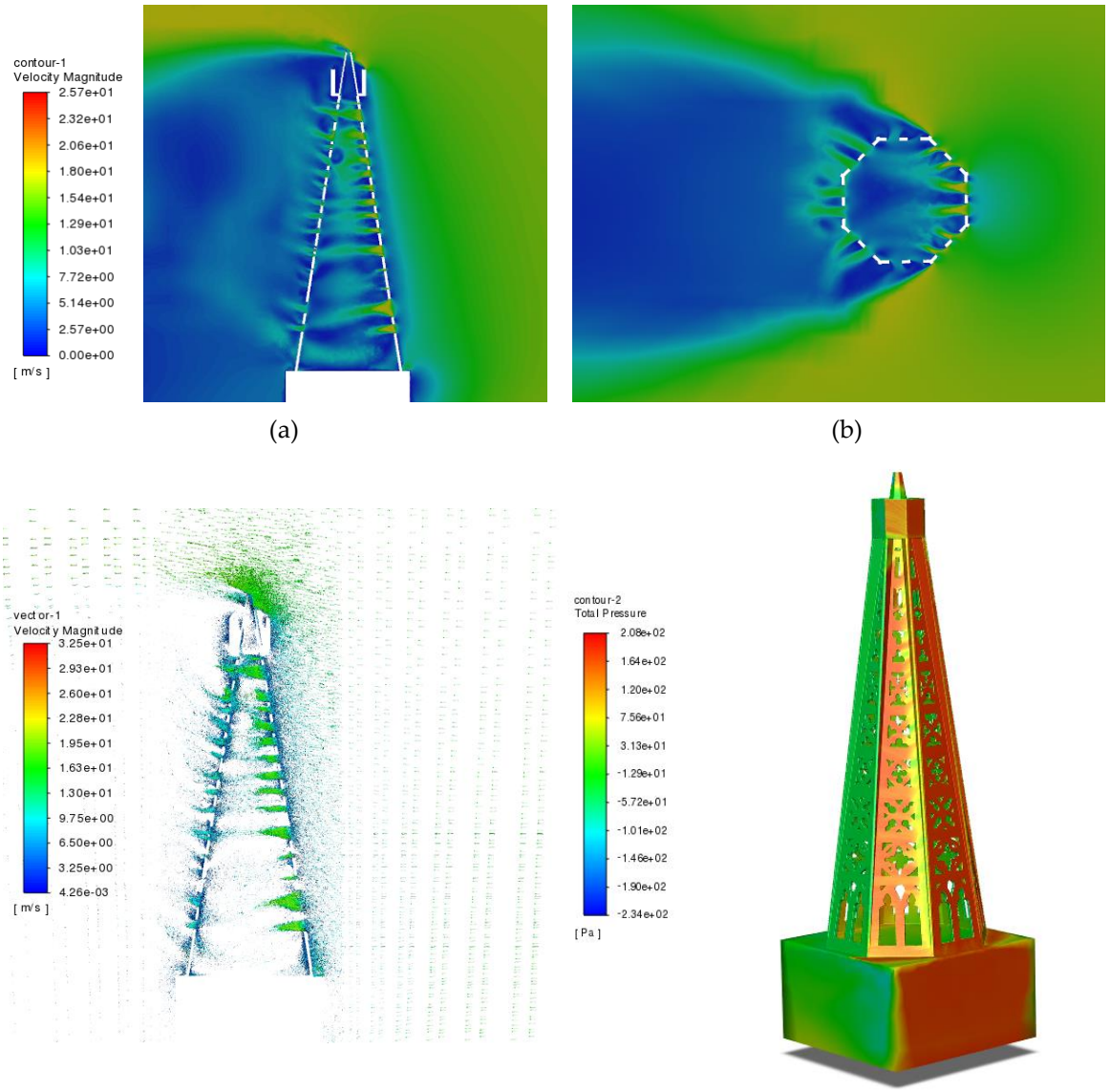

Figure 18. Key results from the CFD model: (a) wind speed distribution – elevation view, (b) wind speed distribution – plan view, (c) wind orientation, and (d) wind pressure on the spire.

From the CFD model results, a mechanical model was developed to determine the horizontal movement of the spire (Figure 19).

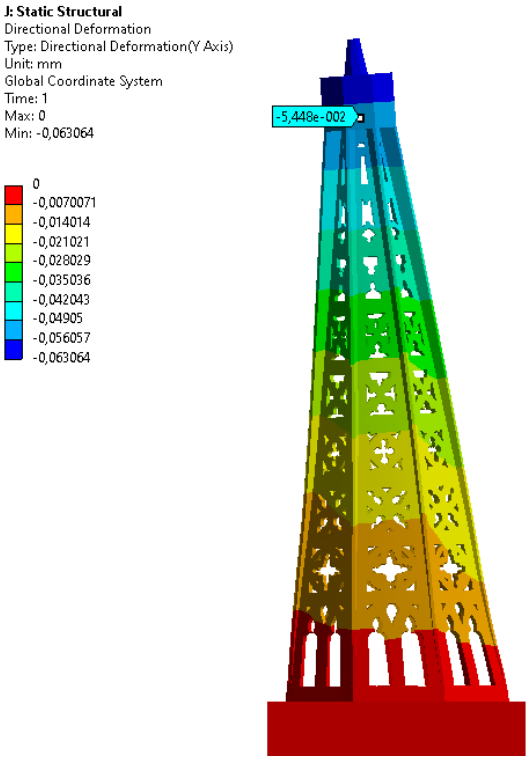

Figure 19. Horizontal movement of the spire caused by wind, as obtained from the FE model.

Figure 19 reveals that the maximum horizontal movement at the point of the spire, where the LVBDT sensor was located was approximately 0.06 mm. This confirms the result, previously deduced from the experimental data, whereby the thermal deformations were larger than those produced by the wind by two orders of magnitude. Consequently, the overall motion of the spire was dominated by thermal actions, whereas low-magnitude, high-frequency wind action was hardly detectable by the LVBDT sensor.

4.4. Induced vibration event

The induced vibration event took place during the ringing of the bells on 25 May, 2021 which lasted approximately 3 min. The two bells were located under the monitored spire. In this case, the thermocouple and anemometer data were not included, as the duration of the event was too short for the temperature and wind to have a significant effect. It should be noted that the average temperature was 17.5 °C and the average wind speed was 5 km/h, with no notable gusts. On the other hand, the accelerations at the base and top of the spire were included (Figure 20).

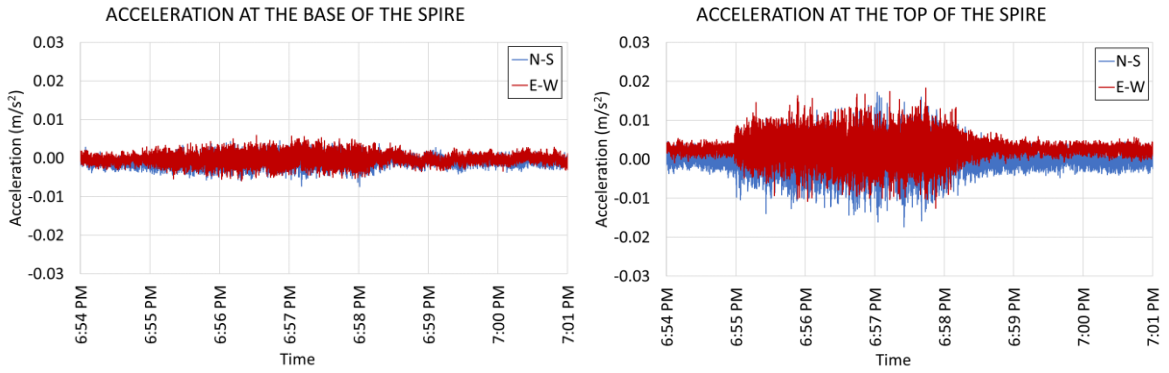

(a) (b)

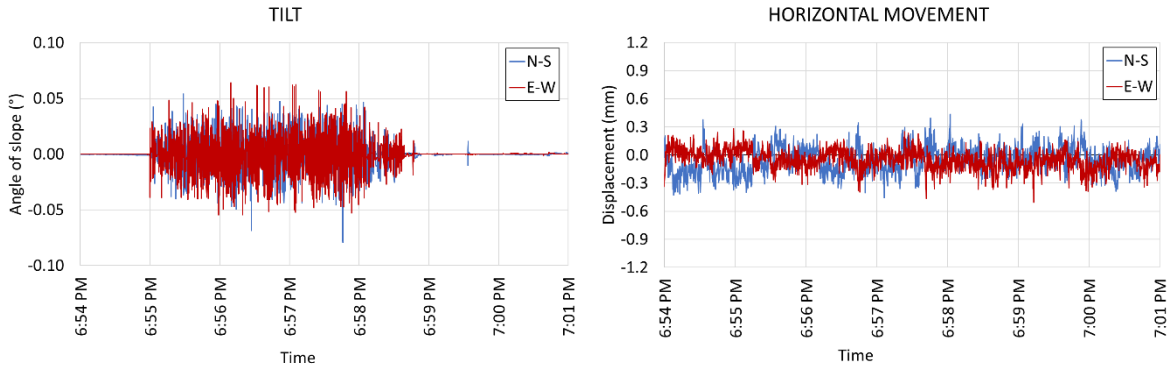

(c) (d)

Figure 20. Measurements during the induced vibration event: (a) acceleration at the base of the spire, (b) acceleration at the top of the spire, (c) tilt, and (d) horizontal movement.

The accelerations at the base and top of the spire are shown in Figures 20a and b, respectively. It can be observed that the vibrations generated by the bells caused much higher accelerations at the apex than at the base. Again, this was to be expected because the behaviour of the spire is equivalent to that of a cantilever, and therefore, the greatest movements and accelerations would occur at its free end. In this case, since it was a short-term measurement, the sampling rate of the accelerometers was 50 Hz.

Figure 20c shows the tilt at the top of the spire. Similar to the case of wind, the bells caused high-frequency vibrations without a predetermined direction. In this event, the amplitude in terms of tils was slightly higher, with an average range of ±0.06°.

Finally, Figure 20d shows the horizontal displacement recorded by the LVBDT. Again, the results reveal that the sensor could not record the high frequency and very low horizontal displacement caused by the ringing of bells. Therefore, it was inferred that the major application of the LVBDT was the monitoring of low-frequency displacements.

Additionally, A DFT was performed on the data recorded by the accelerometer placed at the top of the spire to identify dominant frequencies within the recorded data (Figure 21).

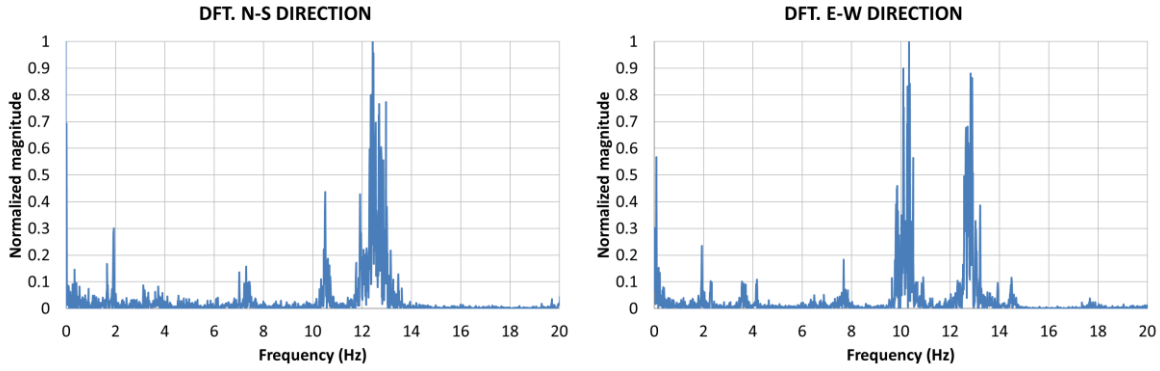

(a) (b)

Figure 21. DFT results from field study: (a) North-South direction, and (b) East-West direction.

Figure 21a shows that, in the N-S direction, the main natural frequency is 12.43 Hz. Another relevant peak frequency can be observed at 10.50 Hz. On the other side, in the E-W direction, the main natural frequency is 10.33 Hz, while the other relevant peak frequency can be observed at 12.83 Hz.

In conclusion, the two most important natural frequencies of vibration of the spire are approximately 10.50 Hz and 12.50 Hz.

In addition, a modal study was conducted to determine the natural frequency of the vibration of the spire. The first mode of vibration corresponded to a frequency of 8.89 Hz and was associated with a cantilever-like behaviour; here, the top of the spire oscillated horizontally (Figure 22). However, the frequency of the ringing of bells was approximately 2 – 3 Hz, which is quite different from the natural frequency. Therefore, as the experimental data showed, the ringing of the bells had a very low dynamic influence on the structure, and the horizontal movements produced were of very low magnitude and practically undetectable for the LVBDT.

A comparison of the theoretical natural frequency (obtained from the FEM) with the measured natural frequencies (see Figure 21) shows that the latter are slightly higher than the former, which reveals that the structure is stiffer than that predicted by the model.

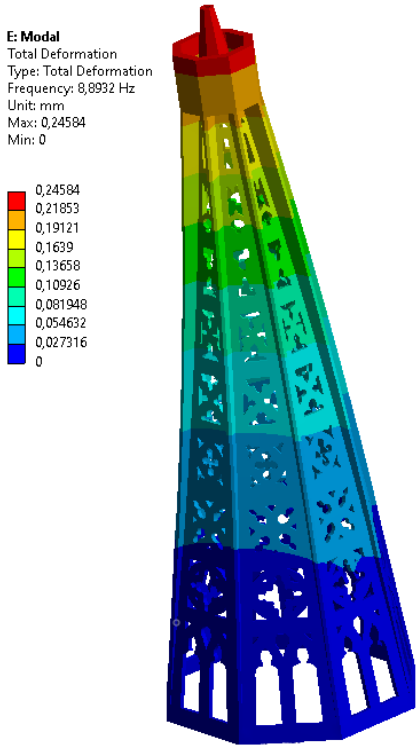

Figure 22. First mode of vibration of the spire and its corresponding frequency, as obtained from the FE model.

Table 3 shows the main dynamic parameters of the spire.

Table 3. Main dynamic parameters of the spire.

Mode	Frequency (Hz)	Period (s)	Participation factor	Ratio	Effective mass	Cumulative mass fraction	Ratio of effective mass to total mass
1	8.89	0.11	6.638	1.000	44.063	0.512	0.459
2	8.89	0.11	3.029	0.456	9.174	0.618	0.096
3	21.14	0.05	0.029	0.004	0.001	0.618	0.000
4	21.27	0.05	0.001	0.000	0.000	0.618	0.000
5	22.23	0.04	5.441	0.820	29.608	0.962	0.308
6	22.24	0.04	1.814	0.273	3.291	1.000	0.034

Table 3 shows that the first mode mobilised a significant part of the total mass (45.9%). The other important mode was mode 5, which mobilised an additional 30.8%. Figure 23 shows the fifth mode of vibration.

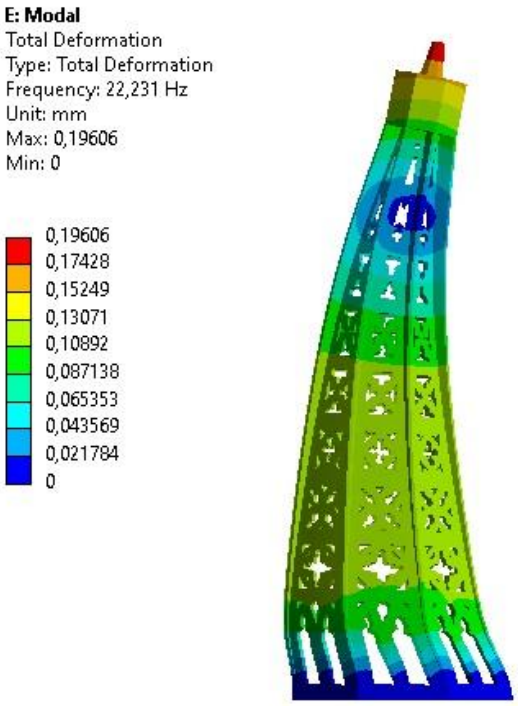

Figure 23. Fifth mode of vibration of the spire and its corresponding frequency, as obtained from the FE model.

4.5. Measurement stability test

In addition to the monitoring of meteorological events, a measurement stability test was also performed. The objective was to check if there was any drift in the LVBDT measurement; in other words, to verify that the measurements remained stable over time. For this purpose, the data recorded by the sensor during the afternoons of 02 April and 12 May, 2021 were compared. These are two meteorologically similar days, with reduced wind and an average temperature of approximately 14 °C. Therefore, the spire was assumed to be in the same position on both the days.

During these 40 days, the measurement algorithm had not been recording constantly; instead it was activated and deactivated numerous times. However, during this entire duration the LVBDT was not manipulated.

Figure 24 shows the horizontal displacement of the top of the spire, as measured on 02 April (Figure 24a) and 12 May (Figure 24b) in 2021, respectively.

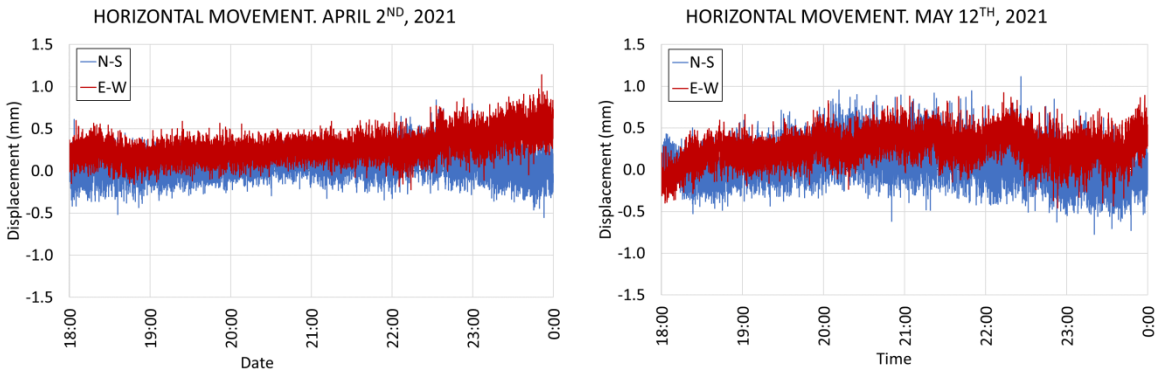

(a) (b)

Figure 24. Horizontal movement measured during two different days: (a) 02 April, 2021 and (b) 12 May, 2021.

Figure 24 shows that the data were very similar. In both the cases, the mean values were practically identical and the oscillation was less than 1.5 mm in either direction.

It can be concluded that the LVBDT provided a robust long-term measurement, as it was able to maintain the stability of measurements for 40 days without any appreciable drift. Furthermore, it was found that as long as neither the fixed nor the mobile part of the sensor was manipulated, it was possible to de-activate the measurement algorithm or even switch off the computer running it. This is a very important aspect, as this is often a limitation of other types of sensors.

5. Summary and conclusions

Significant developments in recent years in the field of machine vision have led to the emergence of a sensor for the measurement of movements based on laser positioning and machine vision, capable of long-term, highly stable, accurate, robust, and cost-effective monitoring of movements as complicated as those occurring at the top of a spire of a cathedral.

Long-term monitoring of horizontal movements in high-rise structures, such as towers or spires of churches or cathedrals, minarets, and chimneys is of great interest because most of the structural degradation phenomena of buildings result in horizontal movement of their tops.

The aim of the current study was to evaluate the robustness of the LVBDT laser positioning and machine vision-based sensor in a real environment, with specific application to the southern spire of the Cathedral of Saint Mary of Burgos, Spain. This structural element was monitored, on an intermittent basis, for more than one year, during 2020–2021; different meteorological events were recorded, and several tests of robustness and accuracy of the measurement system were carried out.

In addition to the LVBDT sensor, numerous conventional back-up sensors, including an inclinometer, accelerometer, a thermocouple, an anemometer and a wind vane were used. Additionally, two numerical models (a CFD model and a mechanical FE model) were employed to correlate the measured responses with the expected theoretical values.

The results from the sensors showed how the spire, given its characteristics, exhibited significant horizontal movements of a thermal nature (variations of up to 4 mm for the thermal variation event). However, the spire hardly suffered any horizontal movement under intense wind events, as it is a very wind-permeable structure, given its shape and numerous openings; furthermore, it hardly exhibited any horizontal movement under induced vibrations (in this case, the ringing of the cathedral bells).

The numerical models also yielded interesting results. Firstly, it was observed that the horizontal movement of the spire was governed by thermal variations, while the action of the wind caused very small displacements, namely, two orders of magnitude smaller. In addition, the first mode of spire vibration occurred at a frequency of 8.89 Hz; as a result, the ringing of the bells (with excitation frequencies below 3 Hz) could not excite the structure; thus, the horizontal movements generated were very small and undetectable by the LVBDT sensor.

The test carried out to measure the white noise of the LVBDT sensor showed that the measurement uncertainty was very low; moreover, it decreased with the reading frequency. This is an important aspect, as in the case of long-term monitoring of slowly developing phenomena (such as those related to structural degradation), the accuracy would be very good (uncertainty of less than ±0.05 mm).

Finally, the test carried out to evaluate the stability of the measurement showed that the measurement was stable in the long term, since two measurements taken 40 days apart and under very similar environmental conditions yielded practically identical values of horizontal movement. This is an essential requisite for long-term monitoring.

It can be concluded that the developed solution yielded excellent field conditions for long-term monitoring of horizontal movements, especially those of slow development, combining very good accuracy, high robustness, good long-term stability, and low cost.

6. Acknowledgments

The authors are grateful for the financial support provided by the University of Burgos, Spain, through the *VII Edition of the Convocatoria Prueba Concepto: Impulso a la valorización y explotación de resultados de investigación* (Acronym: LASARTVIEW). They are also grateful to the chapter of the Cathedral of Saint Mary of Burgos for providing access to the south spire for the work and their logistical support.

7. Patents

A Spanish patent (patent no: ES 2 684 134 B2) was granted [42].

References

[1]. Croci, G. (2000). "General methodology for the structural restoration of historic buildings: the cases of the Tower of Pisa and the Basilica of Assisi". Journal of Cultural Heritage, v. 1, pp. 7-18.

[2]. Lagomarsino, S. (2012). "Damage assessment of churches after L'Aquila earthquake (2009)". Bulletin of Earthquake Engineering, v.10, pp. 73-92.

[3]. Elyamani, A. (2016). "Conservation-oriented structural analysis of the spire of Barcelona Cathedral". International Journal of Materials Science and Applications, v. 5(6-2), pp. 1-9.

[4]. Baraccani, S.; Zauli, L.; Theodossopulos, D.; Silvestri, S. (2020). "Experimental test on a fibre-reinforced scaled cross vault subjected to in-plane shear displacements at the springings". Construction and Building Materials, v. 265, pp. 120305: 1-14.

[5]. Micelli, F.; Cascardi, A. (2020). "Structural assessment and seismic analysis of a 14th century masonry tower". Engineering Failure Analysis, v. 107, pp. 104198: 1-28.

[6]. Radnic, J.; Matesan, D.; Abaza, A. (2020). "Restoration and strengthening of historical buildings: the example of Minceta Fortress in Dubrovnik". Advances in Civil Engineering, v. 2020, pp. 8854397: 1-17.

[7]. Candelas-Gutiérrez, A.; Borrallo-Jimenez, M. (2020). "Methodology of restoration of historical timber roof frames: application to traditional Spanish structural carpentry". International Journal of Architectural Heritage, v. 14(1), pp. 51-74.

[8]. Acikgoz, S.; Soga, K.; Woodhams, J. (2017). "Evaluation of the response of a vaulted masonry structure to differential settlements using point cloud data and limit analyses". Construction and Building Materials, v.150, pp. 916-931.

[9]. Gentile, C.; Guidobaldi, M. Saisi, A. (2015). "Structural health monitoring of a historic masonry tower ". 2015 IEEE Workshop on Environmental, Energy, and Structural Monitoring Systems (EESMS) Proceedings, DOI: 10.1109/EESMS.2015.7175872.

[10]. Blanco, H.; Boffill, Y.; Lombillo, I.; Villegas, L. (2017). "An integrated structural health monitoring system for determining local/global responses of historic masonry buildings". Structural Control and Health Monitoring, v. 25:e2196, pp. 1-20.

[11]. Ferraioli, M.; Lavino, A.; Abruzzese, D.; Avossa, A.M. (2020). "Seismic assessment, repair and strengthening of a medieval masonry tower in southern Italy". International Journal of Civil Engineering, v. 18, pp. 967–994.

[12]. Zhang, Q.; Yang, B.; Liu, T.; Li, H.; Lv, J. (2015). "Structural health monitoring of Shanghai Tower considering time-dependent effects". International Journal of High-Rise Buildings, v. 4(1), pp. 85-90.

[13]. Cigada, A.; Scaccabarozzi, M.; Zappa, E. Visconti, B.M. (2020). "Critical measurement issues in the use of wire potentiometers for the structural health monitoring of slender structures: the

610 case of the Duomo di Milano main spire". Journal of Civil Structural Health Monitoring, v. 10,
611 pp. 119-134.
612 [14]. Gilchrist, R. (2001) "Norwich Cathedral tower and spire: recording and analysis of a cathedral's
613 longue durée". Archaeological Journal, v. 158:1, pp. 291-324.
614 [15]. Marchi, M. (2008). "Stability and strength analysis of leaning towers". Ph.D. Thesis. Università
615 Degli Studi di Parma.
616 [16]. Preciado, A.; Orduña, A.; Bartoli, G.; Budelmann, H. (2015). "Façade seismic failure simulation
617 of an old cathedral in Colima, Mexico by 3D limit analysis and nonlinear finite element
618 method." Engineering Failure Analysis, v. 49, pp. 20-30.
619 [17]. Ferrante, A.; Clementi, F.; Milani, G. (2019). "Dynamic behaviour of an inclined existing
620 masonry tower in Italy". Frontiers in Built Environment, v. 5:33, pp. 1-16.
621 [18]. Gentile, C.; Ruccolo, A.; Canali, F. (2019). "Long-term monitoring for the condition-based
622 structural maintenance of the Milan Cathedral". Construction and Building Materials, v. 228,
623 117101.
624 [19]. Micelli, F.; Cascardi, A.; Aiello, M.A. (2020). "Seismic capacity estimation of a masonry bell-
625 tower with verticality imperfection detected by a drone-assisted survey". Infrastructures, v.
626 5:72, pp. 1-13.
627 [20]. Kouris, E.-G.; Kouris, L.-A.S.; Konstantinidis, A.A.; Karayannis, C.G.; Aifantis, E.C. (2021).
628 "Assessment and fragility of Byzantine unreinforced masonry towers". Infrastructures, v. 6:40,
629 pp. 1-22.
630 [21]. Gentile, C.; Guidobaldi, M.; Saisi, A. (2016). "One-year dynamic monitoring of a historic tower:
631 damage detection under changing environment". Meccanica, v. 51, pp. 2873-2889.
632 [22]. Erkal A. (2017). "Transmission of Traffic-induced Vibrations on and around the Minaret of
633 Little Hagia Sophia". International Journal of Architectural Heritage, v. 11:3, pp. 349-362.
634 [23]. Elyamani, A.; Caselles, O.; Roca, P.; Clapes, J. (2017). "Dynamic investigation of a large
635 historical cathedral". Structural Control and Health Monitoring, v. 24, e1885.
636 [24]. Ruccolo, A.; Gentile, C.; Canali, F. (2021). "Monitoring an iconic heritage structure with OMA:
637 the Main Spire of the Milan Cathedral". Smart Structures and Systems, v. 27(2), pp. 305–318.
638 [25]. Azzara, R.M.; Girardi, M.; Iafolla, V.; Lucchesi, D.; Padovani, C.; Pellegrini, D. (2021). "Ambient
639 Vibrations of Age-old Masonry Towers: Results of Long-term Dynamic Monitoring in the
640 Historic Centre of Lucca". International Journal of Architectural Heritage, v. 15:1, pp. 5-21.
641 [26]. Ehrhart, M.; Lienhart, W (2015). "Image-based dynamic deformation monitoring of civil
642 engineering structures from long ranges". Proc. SPIE 9405, Image Processing: Machine Vision
643 Applications VIII, 94050J.
644 [27]. Ye, X.W.; Dong, C.Z.; Liu, T. (2016). "A review of machine vision-based structural health
645 monitoring: methodologies and applications". Journal of Sensors, v. 2016, pp. 7103039: 1-10.
646 [28]. Feng, D.; Feng, M.Q. (2016). "Vision-based multipoint displacement measurement for
647 structural health monitoring". Structural Control and Health Monitoring, v. 23, pp. 876-890.
648 [29]. Brownjohn, J.M.W.; Xu, Y.; Hester, D. (2017). "Vision-based bridge deformation monitoring".
649 Frontiers in Built Environment, v. 3:23, pp. 1-16.
650 [30]. Spencer, B.F.; Hoskere, V.; Narazaki, Y. (2019). "Advances in computer vision-based civil
651 infrastructure inspection and monitoring". Engineering, v. 5, pp. 199-222.
652 [31]. Dong, C.Z.; Catbas, N. (2021). "A review of computer vision–based structural health
653 monitoring at local and global levels". Structural Health Monitoring, v. 20(2), pp. 692-743.

654 [32]. Shariati, A.; Schumacher, T.; Ramanna, N. (2015). "Eulerian-based virtual visual sensors to
655 detect natural frequencies of structures". Journal of Civil Structural Health Monitoring, v. 5,
656 pp. 457–468.
657 [33]. Schumacher, T.; Shariati, A. (2013). "Monitoring of structures and mechanical systems using
658 virtual visual sensors for video analysis: fundamental concept and proof of feasibility".
659 Sensors, v. 13, pp. 16551–16564.
660 [34]. Brown, N.; Schumacher, T.; Vicente, M.A. (2021). "Evaluation of a novel video- and laser-based
661 displacement sensor prototype for civil infrastructure applications". Journal of Structural
662 Health Monitoring, v. 11, pp. 265-281.
663 [35]. Vicente, M.A.; Gonzalez D.C.; Minguez, J.; Schumacher, T. (2018) "A novel laser- and video-
664 based displacement transducer to monitor bridge deflections". Sensors, v. 18:970, pp. 1-15.
665 [36]. Korumaz, M.; Betti, M.; Conti, A.; Tucci, G.; Bartoli, G.; Bonora, V. Korumaz, A.G.; Fiorini, L.
666 (2017) "An integrated terrestrial laser scanner (TLS), deviation analysis (DA), and finite
667 element (FE) approach for health assessment of historical structures. A minaret case study".
668 Engineering Structures, v. 153, pp. 224-238.
669 [37]. Arias, P.; Herráez, J.; Lorenzo, H.; Ordóñez, C. (2005) "Control of structural problems in
670 cultural heritage monuments using close-range photogrammetry and computer methods".
671 Computers and Structures, v. 83, pp. 1754-1766.
672 [38]. Sapirsten P. (2016) "Accurate measurement with photogrammetry at large sites". Journal of
673 Archeological Science, v. 66, pp. 137-145.
674 [39]. Marcos, R.M.; Esteber, R.M.; Alonso, F.J.; Diaz-Pache, F. (1993). "Características que
675 condicionan el comportamiento de la caliza de Hontoria (Burgos) como piedra de edificación
676 (in Spanish)". Boletín Geológico y Minero, v. 104(5), pp. 587-597).
677 [40]. Cóstola, D.; Clocken, B.; Hensen, J.L.M. (2009). "Overview of pressure coefficient data in
678 building energy simulation and airflow network program". Building and environment, v. 44,
679 pp. 2027-2036.
680 [41]. Defraeye, T.; Carmeliet, J. (2010). "A methodology to assess the influence of local wind
681 conditions and building orientation on the convective heat transfer at building surfaces".
682 Environmental Modelling & Software, v. 25, pp. 1813-1824.
683 [42]. Vicente, M.; González, D.; Mínguez, J. Spanish Patent No. ES 2684134 B2. "Sistema y
684 procedimiento para la monitorización de estructuras (in Spanish)", Award Date: Oct. 3rd, 2019.